

Density-functional theory study of the electronic structure of thin Si/SiO₂ quantum nanodots and nanowires

Pavel V. Avramov,^{1,2,*} Alexander A. Kuzubov,² Alexander S. Fedorov,² Pavel B. Sorokin,^{2,3}
Felix N. Tomilin,² and Yoshihito Maeda^{1,4}

¹Takasaki Branch, Advanced Science Research Center, Japan Atomic Energy Agency, Takasaki 370-1292, Japan

²L.V. Kirensky Institute of Physics, SB RAS, Akademgorodok 660036, Russia

³N.M. Emanuel Institute of Biochemical Physics, RAS, 119334 Moscow, Russia

⁴Department of Energy Science and Technology, Kyoto University, Sakyo-ku, Kyoto 606-8501, Japan

(Received 25 November 2006; revised manuscript received 15 February 2007; published 17 May 2007)

The atomic and electronic structures of a set of proposed pentagonal thin (1.6 nm in diameter) silicon/silica quantum nanodots (QDs) and nanowires (NWs) with narrow interface, as well as parent metastable silicon structures (1.2 nm in diameter), were studied using cluster B3LYP/6-31G* and periodic boundary condition (PBC) plane-wave (PW) pseudopotential (PP) local-density approximation methods. The total density of states (TDOS) of the smallest quasispherical QD (Si₈₅) corresponds well to the PBC PW PP LDA TDOS of the crystalline silicon. The elongated SiQDs and SiNWs demonstrate the metallic nature of the electronic structure. The surface oxidized layer opens the band gap in the TDOS of the Si/SiO₂ species. The top of the valence band and the bottom of conduction band of the particles are formed by the silicon core derived states. The theoretical band gap width is determined by the length of the Si/SiO₂ clusters and describes the size confinement effect in the experimental photoluminescence spectra of the silica embedded nanocrystalline silicon with high accuracy.

DOI: 10.1103/PhysRevB.75.205427

PACS number(s): 73.22.-f, 73.21.Hb, 73.21.La

I. INTRODUCTION

Owing to their potential applications in optoelectronics, the study of silicon nanowires and quantum dots is a very active field of research. Optical properties of these confined systems are known to be quite different from their bulk counterparts and even from each other. The specific role of the surface oxidized layer¹⁻⁷ (or Si/SiO₂ interface) in the formation of the optical properties of the species (see, for example, Ref. 8) has not been studied theoretically yet because of the complexity of the atomic structure of the silica embedded nanocrystalline silicon particles.

Zero- or one-dimensional silicon and silicon-silica quantum dots (QDs) and nanowires (NWs) of various shapes and structures were synthesized under high-temperature conditions (see, for example, Refs. 1-7 and 9-19). The polycrystalline nature of the silicon core of some nanowires was clearly seen^{1,2,9} on the transmission electron microscopy (TEM) images of the species. The bulk-quantity Si nanowires covered by a SiO₂ layer^{1,2} were synthesized by thermal evaporation of powder mixtures of silicon and SiO₂ or by thermal evaporation of silicon monoxide.⁹ The laser ablation in combination with the cluster formation and vapor-liquid-solid growth method¹¹ was used to synthesize the bulk quantities of fine (6-20 nm in diameter) Si/SiO₂ nanowires (1-30 μm in length) using metallic iron as a catalyst. The TEM images demonstrated the perfect crystalline structure of the silicon core, as well as the amorphous nature of the outer silica layer with perfectly round cross section.

In some special cases, the orientation of the main axis (Ref. 20 and references therein) as well as an atomic structure of NW's facets were determined. Mostly,²⁰ the NW's axes are parallel to the [112] direction with (111) facets and in some cases the [110] direction with (100) facets were

detected. The effective diameter of the species²⁰ is in the range of 1.3-7 nm.

The short survey paper¹³ demonstrates a number of perfect silicon NW structures with different sizes and shapes from small round and polygonal cross sections up to square ones for structures with relatively big characteristic thickness. This fact can be explained by a strong surface tension of the thin species that changes the crystalline nature of the SiNWs. For the larger sizes, the surface tension becomes less important and cannot change the cross section of the NWs, which keeps the bulk nature of the atomic structure.

The structure and properties of silicon quantum dots with characteristic diameters from 2 to 10 nm embedded into silica environment were studied, for example, in Refs. 3-7. In contrast with the semiconducting nature of the bulk silicon, the metallic behavior of the columns formed by nanocrystalline silicon (nc-Si) particles was detected.³ Oxidation of the columns leads to the formation of nc-Si (with the characteristic size ~2 nm) superlattice embedded into amorphous silica environment. The metallic conductivity was attributed to the significant structural tension in the interface regions. The decrease of the tension by hydrogen chemisorption or by the creation of the oxidized layer on the surface of the species recovers the semiconducting nature of the silicon nano-objects.

The structure of ultrathin Si(111)/SiO₂ interfaces was studied in Ref. 20 by photoelectron spectroscopy. It was shown that before annealing, the interface thickness is ~2 monolayers of silicon whereas the annealing makes it more abrupt (~1.5 monolayers). The Si 2p x-ray photoelectron spectroscopy spectrum⁶ of the nc-Si quantum dots embedded into the α-SiO₂ matrix [the thickness of the surrounding α-SiO₂ layer is estimated to be ~1.6 nm (Ref. 6)] demonstrates only Si⁺⁴ (SiO₂) and Si⁰ (nc-Si) components. It is a

direct evidence of the real sharpness of the interface.

The photoluminescence (PL) properties of the nanosized silicon were widely studied in the literature (see, for example, Refs. 6–8 and 21–30 including a detailed review²¹). The strong size confinement dependence of the PL photon energy upon the effective size of the nc-Si parts (or, exactly speaking, upon the confinement parameter $1/d$, where d is the characteristic size of the nc-Si parts) was demonstrated for nanocrystalline silicon from 1 nm (Ref. 22) and up to 9 nm (Ref. 7). For the different samples, the PL photon energy can vary from 2.30 eV [1 nm (Ref. 22)] and up to 1.28 eV [4.5 nm (Ref. 24)]. It was shown that the role of surface effects in the determination of the PL properties of the nc-Si structures is really important.^{8,23,28,31}

The luminescence properties of the silicon nanowires have been studied experimentally less extensively.^{29,30} It was shown²⁹ that the quantum confinement effect increases the width of the band gap from 1.1 eV (bulk silicon) up to 1.56 eV (NWs). The electroluminescence peak with the energy of 600 nm (2.07 eV) (Ref. 30) came from silicon nanowires with average diameter of 4 nm as a result of band-to-band electron-hole recombination.

Some possible pristine zero-dimensional (0D) and one-dimensional (1D) silicon nanostructures without saturation of the silicon surface dangling bonds were studied theoretically^{32–39} using a set of *ab initio* electronic structure methods and molecular-dynamics simulations. The atomic structure of the most promising small 0D and 1D polygonal nano-objects was proposed in Refs. 32 and 35 based on the tetrahedral or 1D trigonal prism fragments of the bulk silicon selected along the [110] direction. In the calculations, a rearrangement of the surface of the objects due to dimer formation was found. The density-functional theory (DFT) electronic structure calculations of the 1D silicon structures reveal the metallic or semimetallic nature of the electronic structure of the objects.^{36,38}

The atomic and electronic structures of 0D and 1D silicon structures covered by hydrogen were studied in Refs. 32 and 39–49 using tight-binding (TB),^{40,43,44} empirical Hamiltonian direct diagonalization,³⁹ and local-density approximation^{32,41,42,45–49} (LDA) approaches. To calculate optical properties, the effective mass approach,^{39,43} dipole approximation^{42,44} Green's wave function,^{47,49} and time dependent DFT (Refs. 46 and 48) approximations were used. The atomic models of the 0D and 1D species were based on the crystal structure of bulk silicon with square or rectangular cross sections. All electronic structure calculations demonstrate a semiconducting forbidden gap and describe well the quantum confinement effect.

The study of the role of surface oxygen in the electronic structure of the nc-Si was performed less extensively (see Refs. 8 and 50–53). The electronic structure of some small silicon clusters covered by hydrogen with one Si=O bond on the surface was calculated using cluster LDA approach only in Ref. 8. Based on the LDA results, some large silicon structures (~ 5 nm effective size) covered by hydrogen with one Si=O bond on the surface were calculated using the TB approach. Even one single surface Si=O bond leads to a considerable redshift of the band gap in the electronic structure of the objects.

As it has been shown in the Introduction, no realistic atomic models of the Si/SiO₂ quantum dots and nanowires with narrow Si/SiO₂ interfaces—taking into account the silica environment of the nc-Si core—have been developed and studied by *ab initio* technique. This is in spite of the electronic structure of pristine silicon and hydrogen passivated silicon nanostructures studied in detail through a set of experimental and theoretical approaches. A molecular design of the Si/SiO₂ quantum dots and nanowires combined with *ab initio* DFT and LDA calculations of the species, using the cluster and periodic boundary condition (PBC) approximations, is the main goal of the present paper.

II. OBJECTS UNDER STUDY AND METHODS OF THE ELECTRONIC STRUCTURE CALCULATIONS

According to Ref. 35, the pentagonal SiNWs are the most stable nanowires among all 1D structures with small diameter, constituted by several silicon prisms cutout along the [110] direction. This important theoretical result can be indirectly confirmed by scanning tunneling microscopy images (Ref. 13 and references therein) of thin SiNWs which have almost polygonal or spherical shapes (in contrast with the middle-size or thick particles which reveal the square or rectangular cross sections¹³). Due to these facts, we used the thin pentagonal silicon nanowires³⁵ as the background to develop the atomic models of silicon and silicon/silica 1D nanostructures with (100) silicon facets and the main axis parallel to the [110] direction.²⁰ To study the electronic structure of the objects and to understand the role of oxidized surface layer, we performed the electronic structure calculations of the species in cluster and PBC approximations.

Like in Ref. 35, the silicon nanowires and nanoparticles with pentagon cross section were designed by cutting out the prisms along the [110] direction from the bulk silicon with one (100) and two {111} planes forming a nearly $2\pi/5$ angle. Therefore, with little shear strain and inexpensive {111} stacking faults, five such prisms can form a pentagonal wire, where all (100) facets permit low-energy reconstruction with characteristic dimer-row pattern.

All designed 1D silicon clusters (Fig. 1) have the same diameter (1.2 nm). The nanoclusters in Fig. 1 are presented in two projections. In comparison, a fragment of ideal crystalline structure of silicon [Fig. 1(a)], calculated using LDA plane-wave (PW) pseudopotential (PP) PBC approximation, is presented. The silicon nanoclusters contain 85 [Fig. 1(b)], 145 [Figs. 1(c) and 1(d)], and 265 [Figs. 1(e) and 1(f)] atoms. To decrease the surface tension of the last structures [Figs. 1(c)–1(f)] cap-shaped structure of the tips was formed by cutting the silicon prisms along the [110] directions from both sides of the wires with formation of correspondent {111} surfaces. The length of the clusters is equal to 1.3, 1.8, and 3.7 nm, correspondingly. The 145 and 265 atom structures can form two types of surface dimers perpendicular to the main axis of the nanowires with the decreasing [Figs. 1(c) and 1(e)] and increasing [Figs. 1(d) and 1(f)] of the surface. The PBC calculations were performed using two slab models [Figs. 1(g), the low surface isomer, and Fig. 1(h), the high surface isomer] with 30 atoms each, developed based on the results of the cluster calculations.

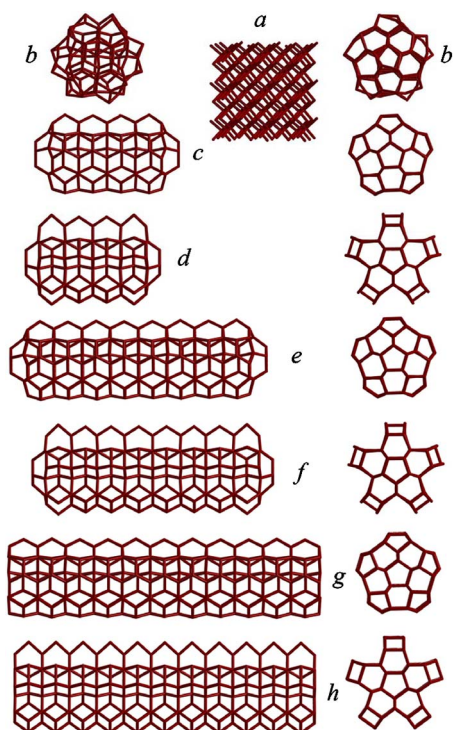


FIG. 1. (Color online) Atomic structure of the pristine silicon 0D and 1D nanoclusters. (a) The fragment of the silicon crystal. (b) Two projections of the Si_{85} quantum dot. (c) Two projections of the low-energy Si_{145} elongated nanocluster. The surface dimers are formed perpendicular to the main axis of the nanocluster to reduce the surface of the object. (d) Two projections of the high-energy Si_{145} elongated nanocluster. The surface dimers are formed perpendicular to the main axis of the nanocluster to increase the surface of the object. [(e) and (f)] Two projections of the low- and high-energy Si_{265} elongated nanoclusters with decreasing and increasing of the surface of the object. [(g) and (h)] Two projections of the low- and high-energy silicon infinite (Si_{30} unit cells) nanowires with decreasing and increasing of the surface of the object.

The atomic structure of the Si/SiO_2 nanoclusters was designed by connecting the silicon atoms with dangling bonds on the (100) surface of the silicon core by bridged oxygen atoms. In Fig. 2, all Si/SiO_2 clusters are presented in two projections, as well as a fragment of crystal lattice of α -quartz. The $\{111\}/(100)$ edges of different silicon prisms were connected to each other by the SiO_2 fragments with bridged silicon atoms between the SiO_2 fragments. For the thin Si/SiO_2 nanowires, the structural tension of the Si/SiO_2 interface is not large because of the relatively good matching of the structural parameters of silicon surface and $\text{Si}-\text{O}$ chemical bonds. Such model of the Si/SiO_2 interface allows all surface related silicon atoms to keep the coordination number 4 which is natural to the SiO_2 oxide. The Si/SiO_2 interface of the caps of finite clusters was designed based on the same model. Due to the shape of the silicon core, each cap has five silicon atoms with three $\text{Si}-\text{O}$ bridged bonds. We guess that this fact is not critical for our study. It is well known (see, for example, Ref. 54 and references therein) that silicon-oxygen clusters often have nonstoichiometric composition.

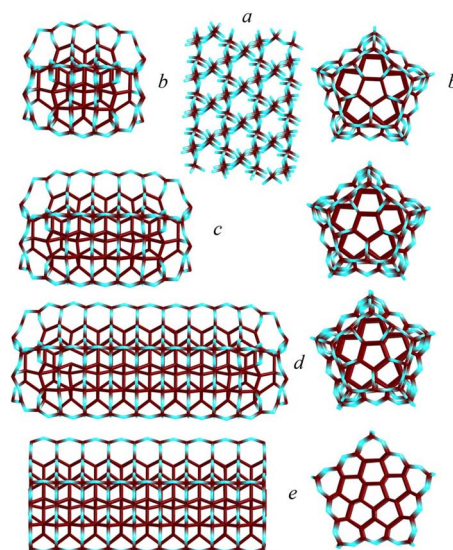


FIG. 2. (Color online) Atomic structure of the silicon/silica 0D and 1D nanoclusters. (a) The fragment of the bulk α -quartz crystal. (b) Two projections of the $\text{Si}_{125}\text{O}_{105}$ quantum dot. (c) Two projections of the $\text{Si}_{195}\text{O}_{145}$ elongated cluster. (d) Two projections of the $\text{Si}_{335}\text{O}_{225}$ elongated cluster. (e) Two projections of the silicon/silica infinite nanowire (the $\text{Si}_{36}\text{O}_{20}$ unit cell). The silicon atoms are presented in darker shade whereas the oxygen atoms are presented in lighter shade.

The coverage of the smallest silicon cluster (85 silicon atoms) by oxidized layer leads to Si/SiO_2 structure with 230 atoms [$\text{Si}_{125}\text{O}_{105}$, Fig. 2(b)]. The elongated Si/SiO_2 clusters contain 340 [on the base of initial Si_{145} cluster, $\text{Si}_{195}\text{O}_{145}$, Fig. 2(c)] and 560 [on the base of initial Si_{265} cluster, $\text{Si}_{335}\text{O}_{225}$, Fig. 2(d)] atoms. For the PBC calculations, the slab model with 56 atoms [$\text{Si}_{36}\text{O}_{20}$, Fig. 2(e)] was chosen.

To calculate the electronic structure of silicon and Si/SiO_2 nanoparticles in cluster approximation, the GAMESS (Ref. 55) code was used. With one exception, the electronic structure calculations of all clusters including geometry optimization were performed at the B3LYP/6-31G(d) level of theory⁵⁶ (from 1615 up to 5880 basis set functions or 4520–14 200 primitive Gaussians for the set of clusters described above) and using the analytic energy gradients. For the $\text{Si}_{335}\text{O}_{225}$ cluster, the atomic structure optimization was performed at the B3LYP/3-21G(d) level (8390 basis functions or 14 430 primitive Gaussians) and finally the density of states (DOS) of the species was calculated using the 6-31G(d) basis set (9740 basis functions or 23 720 primitive Gaussians). The closed-shell electronic structure calculations of all structures except the Si_{85} cluster were performed using the D_{5h} point group of symmetry. For the smallest Si_{85} structure, no symmetry restrictions were used because of possible pronounced distortion of the system by the surface tension. Plots of the calculated DOS were obtained using a broadening energy parameter of 0.1 eV. The resulting band gaps have been extracted as the energy difference between two points of the DOS with intensities less than 0.1%.

The LDA approximation has previously been successfully used to describe the electronic structure of the silicon periodic systems (see, for example, Refs. 32, 36, and 57). To

compare the electronic structure of 1D periodic systems with literature data, we used the LDA approach to compute the electronic structure of the species within the PBC approximation. For all PBC calculations, the Vienna *ab initio* simulation package^{58,59} (VASP) was used. The total-energy code is based on LDA approximation^{60,61} with the Ceperley-Alder exchange-correlation functional,⁶² PW basis sets, and ultrasoft PPs.⁶³ The pseudopotentials allow one to significantly reduce the maximal kinetic-energy cutoff without loss of accuracy. To calculate the electronic structure of all periodic systems, we used 128 points of the k space with $E_{\text{cutoff}} = 250$ eV. All electronic structure calculations of the infinite silicon and silicon/silica nanowires and bulk silicon and α -quartz as well were performed within the PBC approximation (LDA PW PP PBC) without symmetry restrictions of the unit cells. The geometry optimization was carried out until the forces acting on all atoms became lower than 0.05 eV/Å. The same procedure to build up the DOSs and extract the band-gap values, as was described above for the cluster calculations, has been used.

III. RESULTS AND DISCUSSION

A. Pristine silicon structures

The main factor affecting the atomic structure of the thin silicon nanowires is the surface tension caused by dangling bonds on the surface of the objects. The initial atomic structure of the smallest Si_{85} cluster was created using five triangular prisms by the procedure described in the previous section. The surface tension [the B3LYP/6-31G* optimized atomic structure, Fig. 1(b)] leads to a formation of close to spherical Si_{85} quantum dots, keeping the pentagonal nature of the cluster with mirror symmetry along the xy plane.

Taking into account a conservation of the symmetry of the smallest cluster, the atomic structure optimization of all other silicon clusters was performed using the D_{5h} symmetry restrictions. As it was mentioned above, the surface relaxation of crystalline silicon occurs through the formation of the surface dimers. For the 1D silicon structures, there are two ways of dimer formation: parallel and perpendicular to the main axis. In the case of parallel formation of dimers, the atomic structure of the clusters becomes unstable and undergoes fragmentation on small spherical particles (85+60 atoms, for example) during atomic structure optimization. The main reason of the fragmentation is an involvement of tip silicon atoms into the dimer formation process.

The dimer formation perpendicular to the cluster's main axis with the decreasing of the surface of silicon nanostructures [Figs. 1(c) and 1(e)] leads to the low-energy isomers, whereas the increasing of the surface [Figs. 1(d) and 1(f)] leads to the high-energy isomers. On the B3LYP/6-31G* level, the first Si_{145} isomer is (0.05 eV/atom) energetically preferable than the second one. For the Si_{265} pair, this difference is bigger (0.08 eV). In both cases, the tip's atoms of the clusters are not involved in the dimer formation process. Because of this, the bigger the length of the clusters, the bigger the energy difference between isomers.

The optimization of the atomic structure of the infinite silicon nanowires made by LDA PW PP PBC calculations

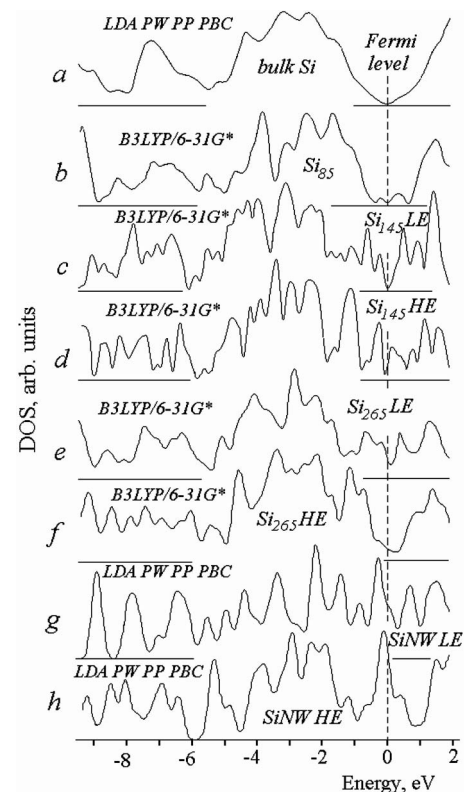


FIG. 3. (a) The LDA PW PP PBC DOS of crystalline silicon. (b) Si_{85} B3LYP/6-31G* DOS. (c) The B3LYP/6-31G* DOS of the low-energy (LE) isomer of the elongated Si_{145} cluster. (d) The B3LYP/6-31G* DOS of the high-energy (HE) isomer of the elongated Si_{145} cluster. (e) The B3LYP/6-31G* DOS of the low-energy isomer of the elongated Si_{265} LE cluster. (f) The B3LYP/6-31G* DOS of the high-energy isomer of the elongated Si_{265} HE cluster. (g) The LDA PW PP PBC DOS of the low-energy isomer of the infinite pristine silicon nanowire. (h) The LDA PW PP PBC DOS of the high-energy isomer of the infinite pristine silicon nanowire.

without symmetry restrictions confirms the results of cluster B3LYP/6-31G* calculations. The atomic structure of the low-energy [Fig. 1(g)] and high-energy [Fig. 1(h)] isomers of the thin silicon nanowires was determined. The decreasing of the surface of the nanowires leads to the lowering of the energy of the system. The energy difference between the isomers is equal to 0.1 eV/atom. The considerable increase of this value in comparison with the Si_{145} (0.05 eV/atom) and Si_{265} (0.08 eV/atom) can be explained by the absence of the tips of the objects in the PBC calculations.

The DOSs of the 0D and 1D structures calculated using the B3LYP/6-31G* and LDA PW PP PBC methods as well as the DOS of the infinite silicon crystal (LDA PW PP PBC calculation) are presented in Fig. 3. The DOS of the Si_{85} quantum dot [Fig. 3(b)] is close to the shape of the DOS of crystalline silicon [Fig. 3(a)], but with small finite density of electron states at the Fermi level. The main difference between the DOSs is the presence of two small intensity peaks from both sides of the Fermi level with -0.3 and 0.3 eV energies, respectively. In general, the DOS of the Si_{85} cluster reproduces well (relative peak energies and intensities) the

DOS of the crystalline silicon in wide energy region from -8 up to 2 eV [Figs. 3(a) and 3(b)].

Elongation of the clusters [Figs. 3(c)–3(h)] leads to fundamental changes in the DOSs of the species. All objects have the metallic nature of the electronic structure. The bigger the length of the objects, the higher the DOS at the Fermi level. Only low-energy isomers of Si_{145} and Si_{265} clusters have close energy peak positions in the density of electron states in the energy region from -2.5 to -8 eV. All other structures have completely different DOS shapes. The most fundamental changes of the DOSs can be observed at the Fermi level. This fact clearly demonstrates the leading role of the surface dimers and tension in the formation of metallic conductivity of the silicon species with unpassivated or strained surface.

The caps of the finite species are not involved in the process of dimer formation perpendicular to the main axis of the objects. The bigger the length of the nanoclusters, the smaller the relative weight of the terminal cap structures. The surface dimer structures lead to a considerable distortion of the atomic structure of the silicon clusters (Fig. 1), especially in the case of high-energy isomers. The surface dimer formation and consequent atomic structure distortion of the species are the main reasons of fundamental changes in the electronic structure of silicon 0D and 1D nanostructures.

B. Silicon/silica structures

The DFT and LDA optimizations of the atomic structure of silicon/silica objects clearly demonstrate the stabilization role of the surface oxidized layer. The bridged oxygen atoms on the surface of silicon cores prevent a formation of the silicon dimer structures and considerable distortion of the atomic structure of the silicon cores of the Si/SiO_2 nanoclusters. The parameters of the $\text{Si}-\text{O}$ chemical bonds in α -quartz (the SiO distance is equal to 1.298 Å and the $\text{O}-\text{Si}-\text{O}$ angle is equal to 111.8°) cannot exactly match the unrelaxed (100) surface of silicon. The cluster B3LYP/6-31G* and LDA PW PP PBC methods give practically the same parameters of $\text{Si}-\text{O}$ bonds at the Si/SiO_2 interface. On the pentagon apexes (see both parallel and perpendicular projections of the infinite Si/SiO_2 nanowire, Fig. 2), the $\text{Si}-\text{O}$ bond length is equal to 1.839 Å and the $\text{O}-\text{Si}-\text{O}$ angle is equal to 149.1° . The lengths of two other $\text{Si}-\text{O}$ bonds of the SiO_2 fragments are equal to 1.671 Å with the $\text{O}-\text{Si}-\text{O}$ angle of 126.3° . The bridged $\text{Si}-\text{O}$ bonds that connect the SiO_2 fragments with the (100) silicon surface are equal to 1.684 Å with the $\text{O}-\text{Si}-\text{O}$ angle of 127.4° . Finally, the bond length of the bridged $\text{Si}-\text{O}$ fragments on the (100) silicon surface is equal to 1.72 Å with the $\text{O}-\text{Si}-\text{O}$ angle of 127.5° . So, the $\text{Si}-\text{O}$ bonds deviate from the bulk SiO_2 ones in the ranges 28%–42% (bond lengths) and 13%–33% (bond angles). Nevertheless, the structural strength of the Si/SiO_2 interface allows the existence of the thin 0D and 1D silicon/silica nanoclusters. This cannot be true for the large ones (see the Introduction) due to the large total surface tension caused by mismatching of the silicon and silica crystal lattices.

The total and partial silicon and oxygen DOSs, calculated using the B3LYP/6-31G* and LDA PW PP PBC methods, of

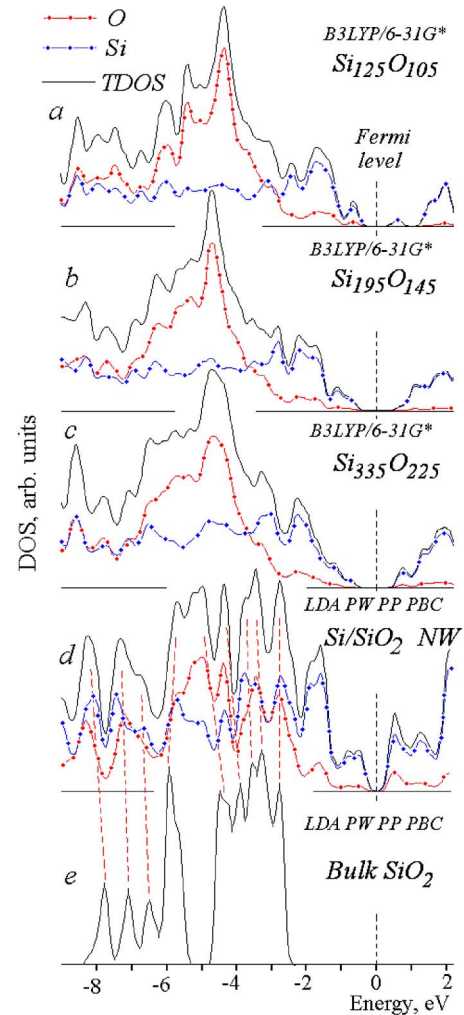


FIG. 4. (Color online) (a) The $\text{Si}_{125}\text{O}_{105}$ quantum dot B3LYP/6-31G* DOS. (b) The B3LYP/6-31G* DOS of the elongated $\text{Si}_{195}\text{O}_{145}$ cluster. (c) The B3LYP/6-31G* DOS of the elongated $\text{Si}_{335}\text{O}_{225}$ cluster. (d) The LDA PW PP PBC DOS of the infinite silicon/silica nanowire. (e) The LDA PW PP PBC DOS of bulk α -quartz. The total densities of states are presented by solid lines. The partial oxygen DOSs are presented by dashed lines with filled circles. The partial silicon DOSs are presented by dashed lines with filled diamonds.

all 0D and 1D Si/SiO_2 species are presented in Fig. 4, as well as one of the α -quartz. All 0D and 1D species have definitely pronounced semiconducting band gaps [Figs. 4(a)–4(d)]. A comparison of the experimental⁷ and cluster B3LYP/6-31G* theoretical data (Table I and Fig. 5) demonstrates an excellent agreement between the B3LYP/6-31G* theory and PL experiment for the elongated Si/SiO_2 clusters of different sizes (1.7–3.8 nm). The theoretical data clearly confirm the size confinement effect^{7,8,22,24,26} shortly described in the Introduction. The band gap of the finite Si/SiO_2 clusters varies from 2.2 eV for the 1.7 nm cluster (230 atoms) up to 1.4 eV for the 3.8 nm cluster (560 atoms). The band gap of the Si/SiO_2 infinite nanowire is equal to 0.6 eV [Fig. 4(d)], which is smaller than the band gap of bulk silicon (1.1 eV) probably due to the well-known underestimation of the semiconducting band gaps by the LDA

TABLE I. Experimental PL (Ref. 7 and reference therein) and theoretical transition energies for the nc-Si/SiO₂ QDs.

Experiment (Ref. 7)			Theory (cluster B3LYP/6-31G*)		
Size (nm)	PL1 (eV)	PL2 (eV)	Size (nm)	First transition (eV)	Second transition (eV)
2.0		1.8–1.9	1.7 × 1.6	1.3	2.2
2.3		1.8	2.3 × 1.6	1.3	1.8
3.8		1.45	3.8 × 1.6	0.8	1.4
4.2	0.9	1.4			

approximation. Comparison of the metallic nature of the pristine Si nanostructures (see previous paragraph and Fig. 3) with the electronic structure of thin Si/SiO₂ 0D and 1D nanoclusters clearly demonstrates the main role of the SiO₂ oxidized layer in the band-gap formation. This effect can be explained by the neutralization of surface dangling bonds and the prevention of surface silicon dimer formation, low-energy position of strongly localized Si—O chemical bonds, and polarization of the electronic structure of the silicon core by negatively charged oxygen ions from the surface oxidized layer.

The excellent agreement between the experimental⁷ and theoretical data for the objects under study can be explained by two reasons. Firstly, even for the smallest Si₁₂₅O₁₀₅ quantum dot, the total number of the basis functions (3950 or 9440 primitive Gaussians, 6-31G* basis set) is good enough for the correct description of the electronic structure of the object. For the large elongated clusters (Si₁₉₅O₁₄₅ and Si₃₃₅O₂₂₅), the corresponding numbers (5880 and 14 200 and 9740 and 23 720) are considerably larger. So, the large total number of the basis functions (or primitive Gaussians) in combination with the hybrid B3LYP DFT potential can be

the main reason for the high accuracy of the DFT calculations of the Si/SiO₂ nanoclusters.

Even the authors of Ref. 7 claimed the spherical shape (or 0D nature) of the nc-Si parts; our DFT calculations of the 1D species describe well the experimental⁷ size confinement effect. It is well known that under the transition from the small clusters to the bulk semiconductors, one can expect a narrowing of the band gap.⁶⁴ In the first approximation, for the elongated systems, the effect can be scaled using two parameters $1/r+1/L$, where r and L are the radius and length of a cluster, correspondingly. At the beginning, for the spherical case, we have the following condition: $r=L$. Because of the equivalence of the r and L coordinates for the spherical case, the energy difference between the occupied and vacant states, derived from the separate r and L parameters, is exactly the same. Elongation of the cluster (increasing of the L value with keeping the r value constant) leads to a splitting of the degenerated electron states at the top of the valence band and the bottom of the conduction band and to decreasing of the energy difference between the electron states, derived by the L value, keeping the r -derived value constant. Since the size confinement effect reflects the inverse dependence of the band gap upon the size of the species, the leading term in the expression is the smallest $1/L$ one, whereas the constant $1/r$ is just a parameter of the system.

The DOS of the infinite Si/SiO₂ nanowire [Fig. 4(d)] in the region from -5 to -8 eV obtained by the LDA PW PP PBC method reflects the shape of α -quartz LDA PW PP PBC DOS [Fig. 4(e)]. Both DOSs have close relative peak intensities and energy positions. This fact can be explained by the localized character and high energy of the Si—O bonds. The top of the valence band (energy region -5 – 0 eV) of all Si/SiO₂ species mainly consists of the Si-derived states of the silicon core (Fig. 4). The conduction band of the infinite Si/SiO₂ nanowire [Fig. 4(d)] contains some small amount of oxygen density near the Fermi level. The analysis of the partial DOSs of the species shows that the Si-derived states of the silicon core near the Fermi level (in both valence and conduction bands) are responsible for the transport and optical properties of the species.

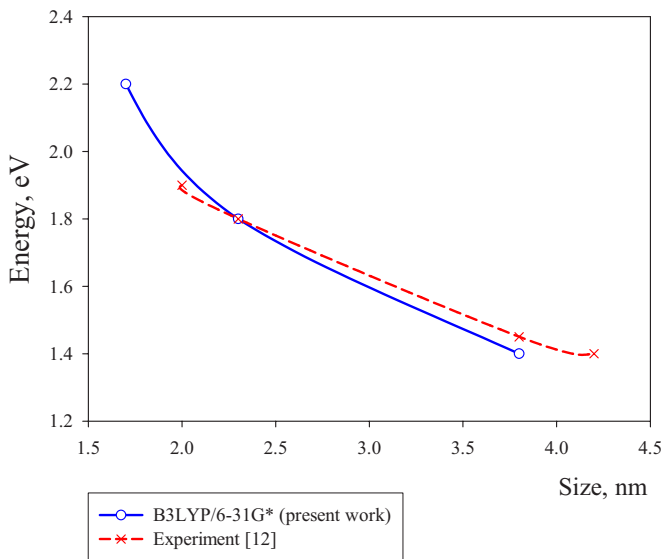


FIG. 5. (Color online) The theoretical B3LYP/6-31G* and experimental (Ref. 7) quantum confinement response of the nc-Si. The dark solid line presents the theoretical B3LYP/6-31G* results, whereas the dashed line presents the experimental data.

IV. CONCLUSIONS

Based on the DFT calculations, we have shown that thin pristine silicon pentagonal nanowires are metastable struc-

tures. The stability of the nanoclusters directly depends on the method of formation of (100) surface silicon dimers. The dimer formation parallel to the main axis of the nanowires leads to a fragmentation of the 1D nanowires and formation of the 0D silicon quantum dots. The metastable silicon 0D and 1D structures have finite density of electron states at the Fermi level. The surface tension and silicon dimers play the dominant role in the formation of the metallic nature of the electronic structure of the silicon nanoclusters. Because of the localized character of the Si—O chemical bonds, the oxidized layer opens an energy band gap in the electronic structure of the Si/SiO₂ nanoclusters, preventing formation of the silicon dimers and decreasing of the surface tension. The DFT calculations clearly confirm the $1/d$ size confinement effect in the optical spectra of the silica embedded nc-Si species with effective size up to 3.8 nm. The Si-derived states of the silicon core determine the optical and transport properties of the silicon/silica objects.

ACKNOWLEDGMENTS

This work was supported in part by the project “Materials Design with New Functions Employing Energetic Beams,” JAEA, JAEA Research Fellowship Program (P.V.A.) and grants from the U.S. Department of Energy via the Ames Laboratory, the Air Force Office of Scientific Research, Russian Foundation for Basic Research (Grant No. 05-02-17443), Deutsche Forschungsgemeinschaft, and Russian Academy of Sciences, No. 436 RUS 113/785 (P.B.S.). The calculations have been partially performed on the Joint Supercomputer Center of the Russian Academy of Sciences. P.V.A. also acknowledges Mark S. Gordon and K.-M. Ho for hospitality during his stay at the Ames National Laboratory (USA) and the personnel of Research Group for Atomic-scale Control for Novel Materials under Extreme Conditions for hospitality and fruitful discussions. The authors also acknowledge Amir Fishman for technical help. The geometry of all presented structures was visualized by ChemCraft software (<http://www.chemcraftprog.com>).

*Corresponding author. FAX: +81 27 346 9670. Email address: avramov.pavel@jaea.go.jp

- ¹N. Wang, Y. H. Tang, Y. F. Zhang, C. S. Lee, and S. T. Lee, *Phys. Rev. B* **58**, R16024 (1998).
- ²N. Wang, Y. H. Tang, Y. F. Zhang, C. S. Lee, I. Bello, and S. T. Lee, *Chem. Phys. Lett.* **299**, 237 (1999).
- ³Q. Chen, X.-J. Li, S. Zhang, J. Zhu, Guien Zhou, K. Q. Ruan, and Y. Zhang, *J. Phys.: Condens. Matter* **9**, L569 (1997).
- ⁴B. J. Hinds, A. Dutta, F. Yun, T. Yamanaka, S. Hatanani, and S. Oda, <http://odalab.pe.titech.ac.jp/PDF/2000/drc.pdf>
- ⁵K. Niguchi and S. Oda, http://odalab.pe.titech.ac.jp/DF/2000/Drc2000_Nishi.pdf
- ⁶Y. Kanemitsu, T. Ogawa, K. Shiraishi, and K. Takeda, *Phys. Rev. B* **48**, 4883 (1993).
- ⁷S. Takeoka, M. Fujii, and S. Hayashi, *Phys. Rev. B* **62**, 16820 (2000).
- ⁸M. V. Wolkin, J. Jorne, P. M. Fauchet, G. Allan, and C. Delerue, *Phys. Rev. Lett.* **82**, 197 (1999).
- ⁹W. S. Shi, H. Y. Peng, Y. F. Zheng, H. Wang, N. G. Shang, Z. W. Pan, C. S. Lee, and S. T. Lee, *Adv. Mater. (Weinheim, Ger.)* **12**, 1343 (2000).
- ¹⁰C. P. Li, X. H. Sun, N. B. Wong, C. S. Lee, S. T. Lee, and B. K. Teo, *J. Phys. Chem. B* **106**, 6980 (2002).
- ¹¹A. M. Morales and C. M. Lieber, *Science* **279**, 208 (1998).
- ¹²X. Duan and C. M. Lieber, *Adv. Mater. (Weinheim, Ger.)* **12**, 298 (2000).
- ¹³D. Appel, *Nature (London)* **419**, 553 (2002).
- ¹⁴J. Heitmann, F. Müller, M. Zacharias, and U. Gösele, *Adv. Mater. (Weinheim, Ger.)* **17**, 795 (2005).
- ¹⁵F. M. Kolb, H. Hofmeister, M. Zacharias, and U. Gösele, *Appl. Phys. A: Mater. Sci. Process.* **80**, 1405 (2005).
- ¹⁶A. Mao, H. T. Ng, P. Nguen, M. McNeil, and M. Meyyappan, *J. Nanosci. Nanotechnol.* **5**, 831 (2005).
- ¹⁷A. Kailer, Y. G. Gogotsi, and K. G. Nickel, *J. Appl. Phys.* **81**, 3057 (1997).
- ¹⁸A. B. Mann, D. van Heerden, J. B. Pethica, P. Bowes, and T. P. Weihs, *Philos. Mag. A* **82**, 1921 (2002).
- ¹⁹J. W. Keiser, J. E. Rowe, J. J. Kolodziej, H. Niimi, H.-S. Tao, T. E. Madey, and G. Lucovsky, *J. Vac. Sci. Technol. A* **17**, 1250 (1999).
- ²⁰D. D. D. Ma, C. S. Lee, F. C. K. Au, S. Y. Tong, and S. T. Lee, *Science* **299**, 1874 (2003).
- ²¹A. G. Cullis, L. T. Canham, and P. D. Calcott, *J. Appl. Phys.* **82**, 909 (1997).
- ²²D. J. Lockwood, Z. H. Lu, and J.-M. Baribeau, *Phys. Rev. Lett.* **76**, 539 (1996).
- ²³S. Schuppler, S. L. Friedman, M. A. Marcus, D. L. Adler, Y.-H. Xie, F. M. Ross, Y. J. Chabal, T. D. Harris, L. E. Brus, W. L. Brown, E. E. Chaban, P. F. Szajowski, S. B. Christman, and P. H. Citrin, *Phys. Rev. B* **52**, 4910 (1995).
- ²⁴O. A. Shalugina, D. M. Zhigunov, M. G. Lisachenko, S. A. Teterukov, D. A. Sapun, V. Yu. Timoshenko, and P. K. Kashkarov, *Physics, Bulletin of Moscow State University (Moscow, Moscow State University, 2005)*, Vol. 1, p. 27.
- ²⁵P. K. Kashkarov, B. V. Kamenev, M. G. Lisachenko, O. A. Shalugina, V. Yu. Timoshenko, M. Schmidt, J. Heitmann, and M. Zacharias, *Phys. Solid State* **46**, 104 (2004).
- ²⁶V. Yu. Timoshenko, M. G. Lisachenko, B. V. Kamenev, O. A. Shalugina, P. K. Kashkarov, J. Heitmann, M. Schmidt, and M. Zacharias, *Appl. Phys. Lett.* **84**, 2512 (2004).
- ²⁷V. Yu. Timoshenko, O. A. Shalugina, M. G. Lisachenko, D. M. Zhigunov, S. A. Teterukov, P. K. Kashkarov, D. Kovalev, M. Zacharias, K. Imakita, and M. Fujii, *Phys. Solid State* **47**, 121 (2005).
- ²⁸J. B. Biteen, N. S. Lewis, H. A. Atwater, and A. Polman, *Appl. Phys. Lett.* **84**, 5389 (2004).
- ²⁹H. Pan, W. Z. Chen, S. H. Lim, C. K. Poh, X. B. Wu, Yu. P. Feng, W. Ji, and J. Y. Lin, *J. Nanosci. Nanotechnol.* **5**, 733 (2005).
- ³⁰J. Huo, R. Solanki, J. L. Freeouf, and J. R. Carruthers, *Nanotechnology* **15**, 1848 (2004).
- ³¹Y. Kanemitsu, S. Okamoto, M. Otobe, and S. Oda, *Phys. Rev. B* **55**, R7375 (1997).

- ³²Y. Zhao, Y.-H. Kim, M.-H. Du, and S. B. Zhang, *Phys. Rev. Lett.* **93**, 015502 (2004).
- ³³B. Marsen and K. Sattler, *Phys. Rev. B* **60**, 11593 (1999).
- ³⁴M. Menon and E. Richter, *Phys. Rev. Lett.* **83**, 792 (1999).
- ³⁵Y. Zhao and B. Yakobson, *Phys. Rev. Lett.* **91**, 035501 (2003).
- ³⁶R. Ruruli and N. Lorente, *Phys. Rev. Lett.* **94**, 026805 (2005).
- ³⁷K. Nishio, T. Morishita, W. Shinoda, and M. Mikami, *Phys. Rev. B* **72**, 245321 (2005).
- ³⁸K. Nishio (private communication).
- ³⁹C.-Y. Yeh, S. B. Zhang, and A. Zunger, *Phys. Rev. B* **50**, 14405 (1994).
- ⁴⁰S. S. Murzin, *JETP Lett.* **55**, 696 (1992).
- ⁴¹F. Buda, J. Kohanoff, and M. Parrinello, *Phys. Rev. Lett.* **69**, 1272 (1992).
- ⁴²M. S. Hybertsen and M. Needels, *Phys. Rev. B* **48**, 4608 (1993).
- ⁴³G. D. Sanders and Y.-C. Chang, *Phys. Rev. B* **45**, 9202 (1992).
- ⁴⁴K. Nishio, J. Kōga, T. Yamaguchi, and F. Yonezawa, *Phys. Rev. B* **67**, 195304 (2003).
- ⁴⁵D. V. Melnikov and J. R. Chelikowsky, *Phys. Rev. B* **69**, 113305 (2004).
- ⁴⁶I. Vasiliev, S. Ögüt, and J. R. Chelikowsky, *Phys. Rev. Lett.* **86**, 1813 (2001).
- ⁴⁷M. Rohlfing and S. G. Louie, *Phys. Rev. Lett.* **80**, 3320 (1998).
- ⁴⁸C. S. Garoufalidis, A. D. Zdetsis, and S. Grimme, *Phys. Rev. Lett.* **87**, 276402 (2001).
- ⁴⁹S. Ögüt, J. R. Chelikowsky, and S. G. Louie, *Phys. Rev. Lett.* **79**, 1770 (1997).
- ⁵⁰A. B. Filonov, A. N. Kholod, V. E. Borisenko, A. L. Pushkarchuk, V. M. Zelenkovskii, F. Bassani, and F. Arnaud d'Avitaya, *Phys. Rev. B* **57**, 1394 (1998).
- ⁵¹A. B. Filonov, S. Ossicini, F. Bassani, and F. Arnaud d'Avitaya, *Phys. Rev. B* **65**, 195317 (2002).
- ⁵²M. Nishida, *J. Appl. Phys.* **99**, 053708 (2006).
- ⁵³M. Nishida, *Phys. Rev. B* **69**, 165324 (2004).
- ⁵⁴P. V. Avramov, I. Adamovic, K.-M. Ho, and M. S. Gordon, *J. Phys. Chem.* **109**, 6294 (2005).
- ⁵⁵M. W. Schmidt, K. K. Baldrige, J. A. Boatz, S. T. Elbert, M. S. Gordon, J. H. Jensen, S. Koseki, N. Matsunaga, K. A. Nguen, S. Su, T. L. Windus, M. Dupuis, and J. A. Montgomery, *J. Comput. Chem.* **14**, 1347 (1993).
- ⁵⁶A. D. Becke, *Phys. Rev. A* **38**, 3098 (1988); C. Lee, W. Yang, and R. G. Parr, *Phys. Rev. B* **37**, 785 (1988).
- ⁵⁷P. Zhang, V. H. Crespi, E. Chang, S. G. Louie, and M. L. Cohen, *Nature (London)* **409**, 69 (2001).
- ⁵⁸G. Kresse and J. Furthmüller, *Comput. Mater. Sci.* **6**, 15 (1996).
- ⁵⁹G. Kresse and J. Furthmüller, *Phys. Rev. B* **54**, 11169 (1996).
- ⁶⁰P. Hohenberg and W. Kohn, *Phys. Rev.* **136**, B864 (1964).
- ⁶¹W. Kohn and L. J. Sham, *Phys. Rev.* **140**, A1133 (1965).
- ⁶²D. M. Ceperley and B. J. Alder, *Phys. Rev. Lett.* **45**, 566 (1980).
- ⁶³D. Vanderbilt, *Phys. Rev. B* **41**, 7892 (1990).
- ⁶⁴Al. L. Efros and A. L. Efros, *Sov. Phys. Semicond.* **16**, 772 (1982).